A simulation workflow for large-scale CO_2 storage in the Norwegian North Sea

Knut-Andreas Lie, Halvor Møll Nilsen, Odd Andersen, Olav Møyner

SINTEF ICT, Department of Applied Mathematics, P.O. Box 124 Blindern, N–0314 Oslo, Norway

Abstract

Large-scale CO_2 injection problems have revived the interest in simple models, like percolation and vertically-averaged models, for simulating fluid flow in reservoirs and aquifers. A series of such models have been collected and implemented together with standard reservoir simulation capabilities in a high-level scripting language as part of the open-source MATLAB Reservoir Simulation Toolbox (MRST) to give a set of simulation methods of increasing computational complexity. Herein, we outline the methods and discuss how they can be combined to create a flexible tool-chain for investigating CO_2 storage on a scale that would have significant impact on European CO_2 emissions. In particular, we discuss geometrical methods for identifying structural traps, percolation-type methods for identifying potential spill paths, and vertical-equilibrium methods that can efficiently simulate structural, residual, and solubility trapping in a thousand-year perspective. The utility of the overall workflow is demonstrated using real-life depth and thickness maps of two geological formations from the recent CO_2 Storage Atlas of the Norwegian North Sea.

Keywords: CCS, vertical equilibrium simulations, spill-point analysis, long-term migration, storage capacity, basin-scale injection

E-mail addresses: Knut-Andreas.Lie@sintef.no (Knut-Andreas Lie)., Halvor.M.Nilsen@sintef.no (Halvor Møll Nilsen)., Odd.Andersen@sintef.no (Odd Andersen)., Olav.Moyner@sintef.no (Olav Møyner).

1. Introduction

The sedimentary basins in the Norwegian North Sea contain a large number of saline aquifers that have small flow rates and offer large volumes of pore space that potentially can be used to store carbon dioxide. In geological carbon storage, CO_2 is injected as a dense phase fluid into a high-permeable strata limited upward by a low-permeable strata (caprock) that inhibits flow. The injected CO_2 has lower density than the formation fluids and will form a separate plume that migrates upward by buoyancy forces. Open aquifer systems are connected to the surface through permeable strata, and injected CO_2 may therefore in principle travel in the up-dip direction and eventually leak back to the atmosphere through sedimentary outcrops. In practice, this process will typically take thousands of years due to the long distances involved. Moreover, as the plume migrates upward, some of the CO_2 will remain behind in structural and stratigraphic traps (structural trapping), be trapped as small droplets between rock grains (residual trapping), dissolve into the formation water (dissolution trapping), or react with rock minerals thereby becoming permanently trapped.

The main concern for policy makers and the general public is risk of leakage: How likely is it that the injected CO_2, or the fluids it expels, will leak to the surface or migrate into active petroleum reservoirs. In other parts of the world, one may also be concerned of leakage of CO_2 or highly saline brine into water resources. In other words, the operator of a potential injection site needs to maximize storage volumes while minimizing leakage risks and undesired effects on areas surrounding the injection points. The operator will obviously also want to ensure operational safety and minimize financial costs. Similar assessments will be desired by companies, investors, and/or government agencies that take an environmental, societal, or financial risk throughout the operation. The only viable way to make such assessments upfront is through model studies that aim to investigate the likely outcomes of a storage operation. Main controls in a model study are the aquifer geology and the physics of the flow processes.

From petroleum exploration and production, it is well known that variations in geological structures and rock properties will strongly impact the migration of hydrocarbons on a basin scale as well as the flow on a reser-

voir scale. Unfortunately, the understanding of most saline aquifers is quite limited: Seismic surveys have limited coverage and few core-samples are available since aquifers seldom have been penetrated by more than a few wells, if any. It is therefore very important that modeling tools are able to properly account for the impact of uncertainty in the geological description of the aquifer to correctly span the range of likely outcomes of an injection operation.

The flow dynamics of the injection and migration processes depend on delicate balances between various physical mechanisms. The balances may vary with spatial location and change significantly as time progresses. Injected, mobile CO_2 can travel long distances, but the flow is typically confined to thin layers underneath the sealing caprock. Because of the high ratio between the lateral and vertical scales involved, and the large disparity in temporal scales of the different physical processes, modeling CO_2 storage is a very challenging multiscale problem that is best attacked using a range of different tools for flow modeling. Whereas traditional tools for 3D simulation can be used to study the buildup of a plume near the injection point, these tools will in most cases not be able to resolve the long-term, large-scale CO_2 migration and the associated trapping processes. Indeed, because the time scale of the vertical flow process is generally much shorter than the time scale of the lateral fluid movement, it is often better, both in terms of accuracy and computational efficiency, to describe the migration process in a vertically-averaged sense on a 2D grid that follows the caprock surface, possibly in combination with invasion-percolation computations and similar ideas that have been developed to study migration processes taking place over millions of years.

Figure 1 gives a conceptual illustration of how different modeling tools and approaches could be used in the various phases of planning a large-scale storage operation. Herein, we will focus on the two first phases: identification of storage potential and placement of injection hubs for large-scale utilization. To this end, we briefly describe a set of simulation tools of increasing computational complexity, and discuss how they can be combined to create a flexible tool-chain for investigating CO_2 storage on a scale that would have significant impact on European CO_2 emissions. In doing so, we consider ideas from computational geometry, basin modeling, hydrology, and reservoir simulation and adapt and combine them in a way that, to the best of our knowledge, is new within CO_2 sequestration modeling. All the tools are implemented in a high-level scripting language as part of the open-

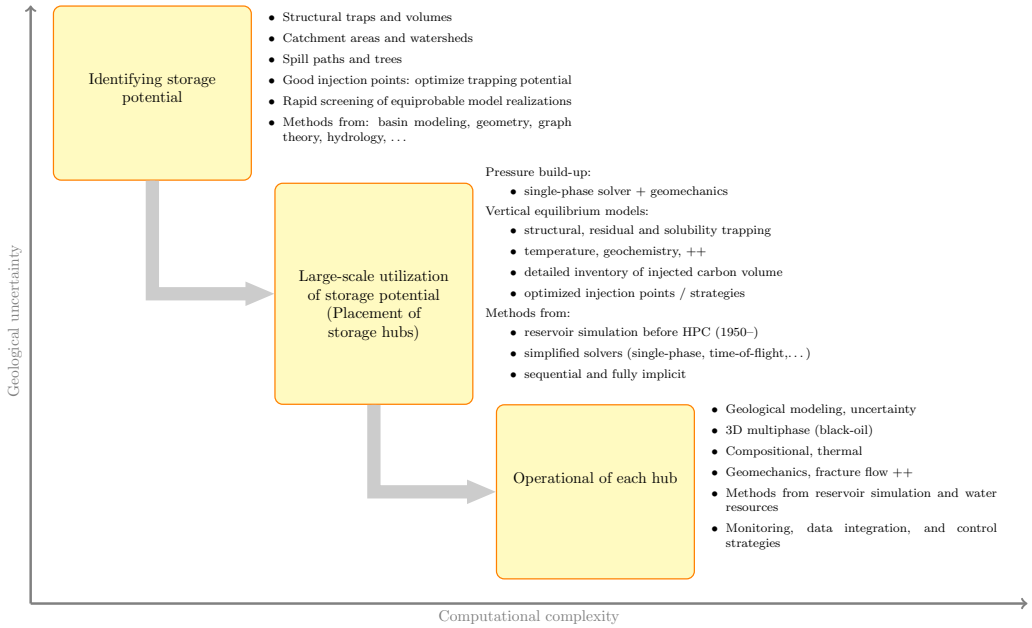

Figure 1: Conceptual picture of how different modeling tools and approaches could be used in the various phases of the planning of a large-scale storage operation.

source MATLAB Reservoir Simulation Toolbox [1, 2], and made available as a separate CO_2 module, [3]. In addition to the methods discussed herein, MRST also implements standard 3D simulation tools: sequential solvers for (in)compressible, immiscible flow, fully-implicit methods based on automatic differentiation for black-oil models (including certain modeling options for enhanced oil recovery), as well as early prototypes of geochemical, thermal, and geomechanical effects.

2. Methodology

All computational methods implemented in MRST-co2lab are formulated based on a hybrid 2D grid that represents the 3D aquifer in terms of its top and bottom surfaces, i.e., the 3D surfaces that separate the high-permeable strata of the aquifer from low-permeable strata that bound it from above and below. These surfaces are represented as depth values at each vertex and edge/cell centroid of a 2D mesh. In addition, each cell in the grid contains information of the petrophysical properties in the volume that lies below it in the 3D representation of the aquifer. The computational methods that

will be discussed in the following can be roughly divided into two classes: (i) methods that do not utilize temporal information to identify the potential for structural trapping [4], and (ii) methods for estimating the outcomes of injection operations in a long-term, large-scale perspective by simulating the combined effects of structural, residual, and solubility trapping in a vertically averaged sense [5, 6]. The methods are designed to fit together as part of a multi-fidelity tool-chain supporting the flexibility in resolution required of simulations used for decision support. Herein, our focus is on workflow tools that enable interactive inspection of models and rigorous mathematical optimization of injection points and strategies.

2.1. Spill-point analysis and structural trapping capacity

In the short term, structural and stratigraphic trapping are the dominant mechanisms for geological storage of CO_2. Structural traps correspond to local maxima in the top surface (see Figure 2), and first-order estimates of the associated storage volumes can be produced quickly by simple geometrical/topological algorithms. In [4], we discuss in detail two variants of such algorithms that use the depth of the top surface evaluated at the cell centers and cell vertices, respectively, to determine *spill paths* connecting each node (i.e., cell or vertex) to its upslope neighbors. Each spill path either ends up in a local maximum or at the perimeter of the model. The top surface may contain one or more closed regions inside which all spill paths converge to a local maximum. These so-called *spill region* act as funnels by collecting buoyant fluids within the area covered by the region and channeling them towards the maximum point. Each spill region is separated topographically from adjacent spill regions, or regions that spill to the exterior of the model, by a perimeter (hydrology: drainage divide or watershed). All nodes situated above the highest point on the perimeter, called the *spill point*, are said to belong to a structural trap (which can potentially be used to safely store CO_2), whereas the remaining part of the spill region is said to belong to the trap's catchment area. Based on this analysis, one can provide upper limits on the amount of CO_2 that may be structurally trapped within an aquifer.

To study migration of CO_2, we can use a percolation-type method that assumes that CO_2 is injected at an infinitesimal rate. In the resulting migration model, CO_2 injected at a point within a catchment area will accumulate inside the associated trap, gradually filling it up until the lower surface of the CO_2 extends down to the spill point. When this happens, CO_2 will en-

ter the adjacent spill region and continue its upward migration towards a new local minimum or the model perimeter. A spill region can obviously be contained within another spill region and/or be linked by spill paths to other non-overlapping spill regions in an upward succession. By nesting the individual spill regions this way, we can define a hierarchical spill system (hydrology: drainage system) that enables us to easily identify potential storage volumes that are upslope of a given point, or vice versa, the catchment areas that are downslope of a point or trap. The upward succession of traps in the spill system can be seen as a set of separate trees (hydrology: drainage basins) that each describe an isolated migration system starting low in the formation at traps (leaf nodes) with no downslope connections and ending up at the root, defined as a trap whose upslope connection is the model perimeter. Using these trees, injection points that are upward connected to large trap volumes can be readily identified. If structural trapping is the only containment mechanism, the best points for finite-rate injections will lie on the perimeter between two (or more) spill regions that are connected upslope to distinctly different trap trees with large and approximately equal trap volumes.

The trapping structure will also influence other trapping mechanisms. In particular, the presence of structural traps will retard the plume migration. Likewise, for the CO_2 to spread out beyond the catchment area in which it is injected, the plume needs to carry sufficient energy to push the CO_2 downward in the formation and across the nearest spill point or the shallowest point on the perimeter. As a result, catchment areas with a strong funneling effect can be expected to reduce and limit the global sweep efficiency. Having a high sweep efficiency is essential if residual effects are to be a viable trapping mechanism.

The primary access in MRST-co2lab to the trapping analysis described above is through a graphical user interface that can be invoked once you have created a proper structure for representing the top-surface grid. However, the software also provides an API to individual functions that implement distinct parts of the analysis, see [4] for more details. All functionality is documented through MATLAB's help system and tutorials that accompany the software.

2.2. Estimation of total trapping capacity

In a long-term perspective, the theoretical storage capacity of an open aquifer cannot simply be defined to equal its pore volume, since open aquifer

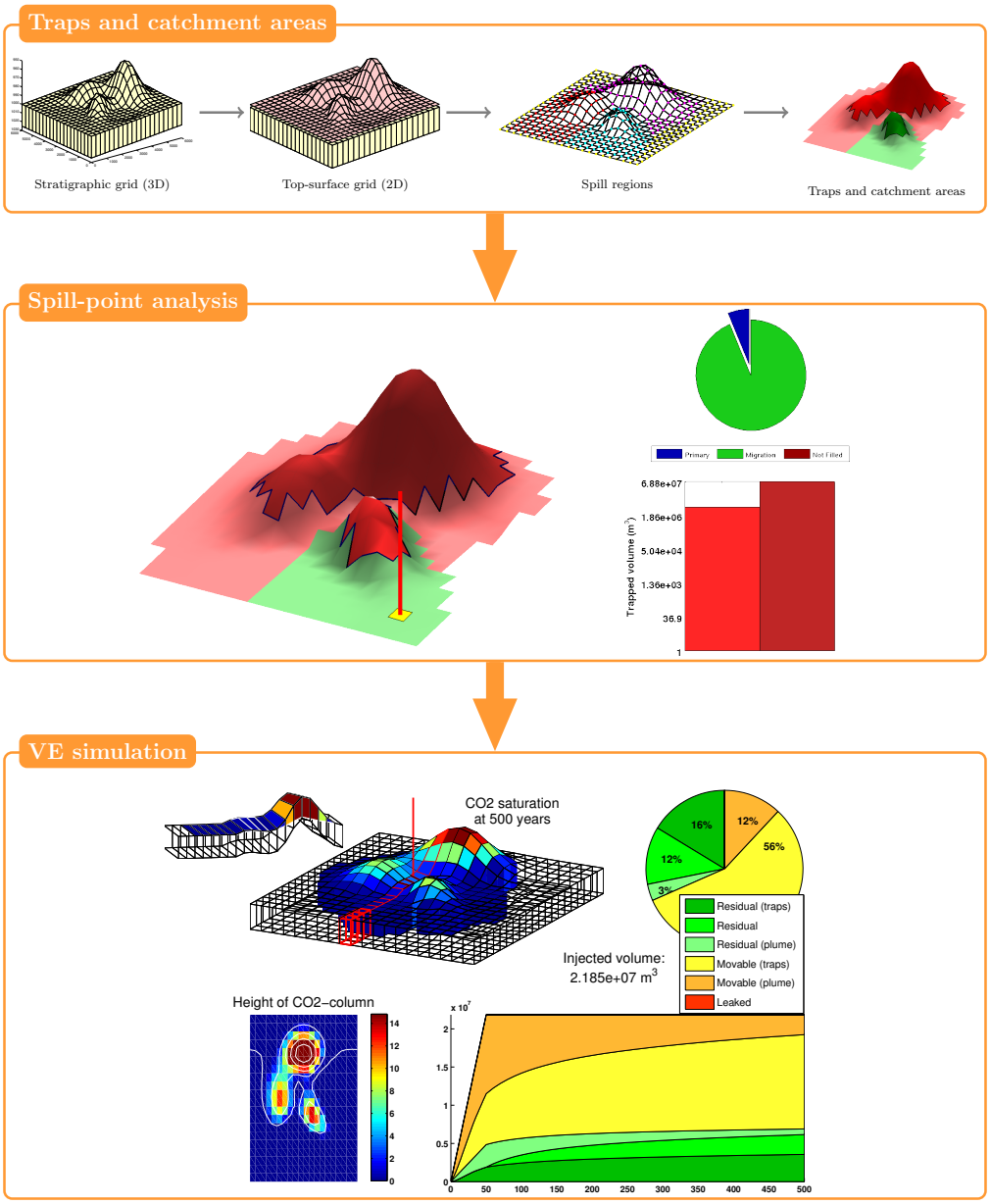

Figure 2: Illustration of the chain of tools implemented in MRST-co2lab.

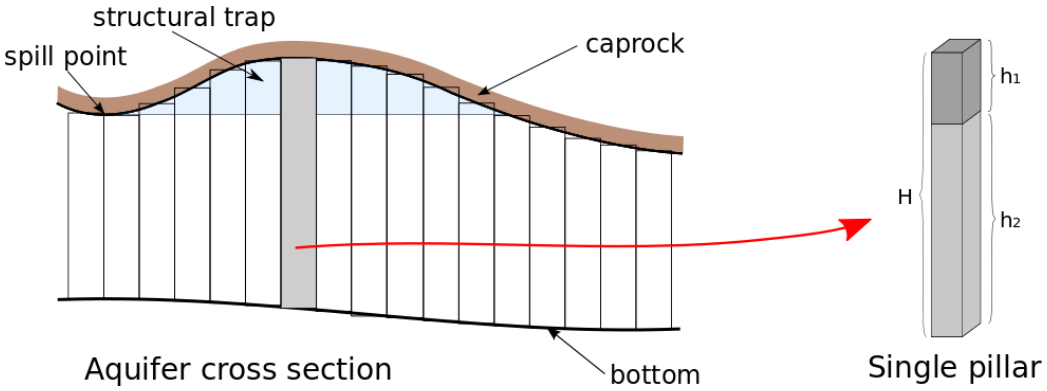

Figure 3: Illustration of how the aquifer volume is divided into a mesh of pillars.

boundaries will not prevent CO_2 from exiting the aquifer and potentially migrate back to the surface. A more useful measure of storage capacity for an open aquifer is therefore the ability of the aquifer to retain CO_2 in the long term through various trapping mechanisms, which we here refer to as its *retaining capacity*. In addition, there are other considerations such as the impact of potential pressure buildup on caprock integrity and the fate of formation water expelled by the invading CO_2. Although highly important, these effects will not be discussed herein.

After structural traps have been identified, the upper bound on the retaining capacity of an aquifer from structural, residual and dissolution trapping can be determined. We approximate the formation geometry as a grid of rectangular, vertical pillars, compute the retaining capacity of each pillar separately, and add up to get the total figure. The height H of a given pillar can be written $H = h_1 + h_2$, where $h_1 (\geq 0)$ represents the part contained within a structural trap, as illustrated in Figure 3.

For the part of the column that lies within a structural trap, the full retaining capacity Q_1 is reached when the pore space is maximally saturated with CO_2 and the remaining brine contains the maximal amount of dissolved CO_2:

$$Q_1 = A h_1 \phi \Big[s_{w,r} c_{max} + (1 - s_{w,r}) \rho_{co_2} \Big]. \tag{1}$$

Here, A is the area of a lateral cross-section of the pillar, ϕ the rock porosity, $s_{w,r}$ the residual water saturation, ρ_{co_2} the CO_2 density, and c_{max} the maximum mass of CO_2 that can be dissolved per volume of formation water. In general, ρ_{co_2} should be considered a function of local temperature and

pressure, which may vary across the aquifer. Assuming hydrostatic conditions and a fixed temperature gradient, temperature and pressure become functions of local depth only.

Similarly, the part of the column not contained within a structural trap is at full retaining capacity Q_2 when all pore space contains the residual amount of CO_2 and all remaining brine contains the maximal amount of dissolved CO_2

$$Q_2 = Ah_2\phi\Big[(1 - s_{n,r})c_{max} + s_{n,r}\rho_{co_2}\Big], \tag{2}$$

where $s_{n,r}$ represents the residual saturation of CO_2.

We now use superscript i to denote a given pillar. The total retaining capacity of pillar i is

$$Q^i = Q_1^i + Q_2^i \tag{3}$$

and the total estimate for the aquifer becomes

$$Q = \sum_i Q^i = \sum_i \left(D^i + S^i + R^i\right) = D + S + R, \tag{4}$$

where

$$\begin{aligned} D^i &= c_{max}\left[h_1^i s_{w,r} + h_2^i(1 - s_{n,r})\right] A\phi, \\ S^i &= \rho_{co_2}^i\, h_1^i(1 - s_{w,r})\, A\phi, \\ R^i &= \rho_{co_2}^i\, h_2^i s_{n,r}\, A\phi. \end{aligned}$$

Here, $D = \sum_i D^i$, $S = \sum_i S^i$, and $R = \sum_i R^i$ represent total CO_2 mass in the aquifer that can be retained by dissolution, structural trapping, and residual trapping, respectively.

2.3. Vertical equilibrium models

Most aquifers considered relevant for carbon storage have spatial extents on the order of tens to hundreds of kilometers in the lateral direction and tens to hundreds of meters in the vertical direction. After injection operations have ceased, the driving forces in the horizontal direction will be moderate and fluid redistribution will mainly be driven by buoyant forces caused by the high density contrast between CO_2 and the resident brine. As a result, the lateral movement of fluids will dominate the large-scale dynamics of the CO_2 plume since the vertical flow takes place on a much shorter time scale. As

a good approximation, the vertical redistribution of fluids can be considered instantaneous so that the fluid phases are always in vertical equilibrium.

This observation naturally leads to a two-scale modeling approach, in which the three-dimensional flow equations are integrated in the vertical direction to form a 2D flow model for the lateral movement of fluids. The effective properties and constitutive relationships that enter the averaged flow equations are in turn determined by hydrostatic phase pressures and analytical expressions that e.g., describe the vertical distribution of fluid phases in vertical equilibrium. This transformation not only reduces the computational cost by reducing the dimension of the problem and increasing the time constants that characterize the dynamics of the model. The analytical expressions also provide an "infinite" vertical resolution, allowing us to describe important parts of the plume dynamics that cannot be accurately resolved by the overly coarse grid resolution that must be imposed vertically to make a 3D model computationally tractable.

For completeness, let us briefly outline the derivation of the most basic form of a vertical-equilibrium (VE) model, which in addition to hydrostatic pressure assumes a sharp interface separating CO_2 and resident brine. To this end, we start with a standard incompressible, two-phase model

$$\frac{\partial \phi s_\alpha}{\partial t} + \nabla \cdot \vec{v}_\alpha = 0, \qquad \vec{v}_\alpha = -\mathbf{k}\lambda_\alpha\big(\nabla p - \rho_\alpha \vec{g}\big). \tag{5}$$

Here, ϕ denotes porosity, $\mathbf{k}$ permeability, p pressure, and $\vec{g}$ the gravity vector, whereas s_α, ρ_α, and λ_α denote saturation, density, and mobility for phase $\alpha = \{w, n\}$. Brine is assumed to be the wetting phase and CO_2 the non-wetting phase, and these two fluids fill the pore space completely so that $s_w + s_n = 1$.

We consider the aquifer to be bounded above and below by impermeable strata separated a distance H. To keep the presentation as simple as possible, we assume that the top surface is planar and slightly inclined and choose our coordinate system such that the z-axis is perpendicular to the top surface and makes a small angle with $\vec{g}$, see Figure 4. Moreover, we assume that ϕ and $\mathbf{k}$ are constant in the z-direction. The general case with an undulating top surface and non-constant petrophysical parameters is discussed in detail in [5] along with certain geometrical approximations that are tacitly introduced in the following. By integrating (5) from 0 to H in the z-direction we obtain

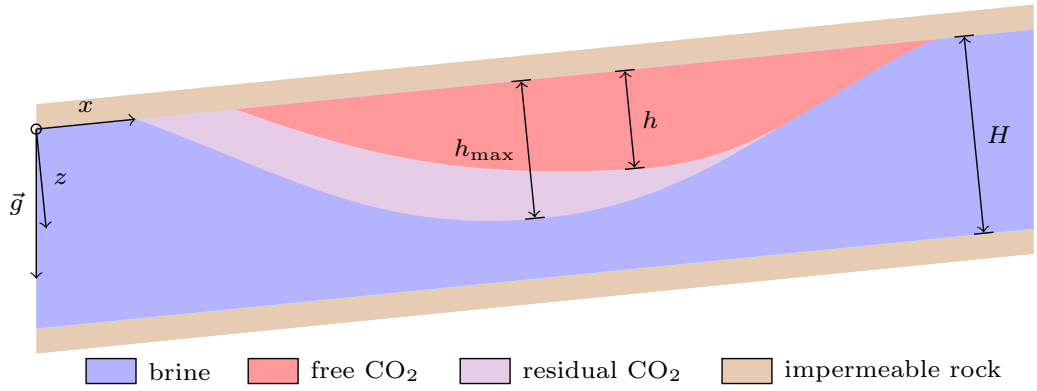

Figure 4: Schematic of the fluid distribution and the coordinate system used to derive the basic vertical-equilibrium model.

the coarse-scale flow equations:

$$\frac{\partial \Phi S_\alpha}{\partial t} + \nabla_\parallel \cdot \vec{V}_\alpha = 0, \qquad \vec{V}_\alpha = -\mathbf{K}\lambda_\alpha(\nabla_\parallel P - \rho_\alpha \vec{g}_\parallel), \tag{6}$$

where $\nabla_\parallel$ denotes a 2D operator, $\vec{g}_\parallel$ is the gravity component in the (x, y)-plane, and upper-case symbols denote upscaled counterparts of quantities denoted by lower-case symbols in (5). From (6) one can easily derive a coarse-scale system formulated in terms of P and one of the phase saturations. To determine the constitutive relations entering (6) we need to determine the fluid distribution along the z-axis. First of all, the fluid distribution is assumed to consist of three zones separated by sharp interfaces: CO_2 with residual brine at the top, brine with residual CO_2 below in a zone from which the CO_2 plume has retracted, and pure brine at the bottom:

$$s(z) = \begin{cases} s_{w,r}, & 0 \le z \le h, \\ 1 - s_{n,r}, & h < z \le h_{\max}, \\ 1, & h_{\max} \le z \le H. \end{cases} \tag{7}$$

Moreover, if we take P to be the pressure at the top surface, the hydrostatic pressure reads

$$p(z) = \begin{cases} P + \rho_n g z, & 0 \le z \le h, \\ P + \rho_n g h + \rho_w g(z - h), & h < z \le H. \end{cases} \tag{8}$$

Then, by simple integration we obtain the following relations between h and $h_{\max}$ and the coarse-scale quantities:

$$\begin{aligned} S_n(h, h_{\max}) &= (1 - s_{w,r})\frac{h}{H} + s_{n,r}\frac{h_{\max} - h}{H} \\ \Lambda_n(h) &= \lambda_n(s_{w,r})h \\ \Lambda_w(h, h_{\max}) &= \lambda_w(1 - s_{n,r})\frac{h_{\max} - h}{H} + \lambda_w(1)\frac{H - h_{\max}}{H} \end{aligned} \tag{9}$$

From this expression, we see that the natural variables to use for the upscaled equations are h and the hysteretic parameter $h_{\max}(t) = \max_{t' \leq t}(h(t'))$. The model can also be formulated using S as a primary unknown, but then we must always invert the functional form of S to compute h before we can determine the relative mobilities. Finally, we notice that the upscaled model will have hysteretic behavior even if the fine-scale model has not.

In MRST-co2lab we have implemented several types of two-phase VE models [5, 6], ranging from the simple sharp-interface model outlined above, which can only account for the basic dynamics of structural and residual trapping, to quite sophisticated models that account for compressibility, fine-scale capillary forces, dissolution, hysteretic effects, subscale caprock trapping, etc. The simplest models are formulated both in terms of h and S and discretized and solved using a sequential splitting method to give high computational efficiency. The more sophisticated methods are, unlike most other VE models reported in recent literature [7, 8, 9, 10, 11], formulated in terms of S using the black-oil framework that is standard in the petroleum industry. To ensure maximum robustness, the models are discretized and solved using a fully-implicit solver [12, 13] as implemented in leading commercial reservoir simulators (e.g., including standard techniques to safeguard the time steps). The fully-implicit solver is implemented using automatic differentiation [14], which enables simple computation of parameter sensitivities and gradients that can be used for mathematical optimization.

3. Large-scale Carbon Storage in the North Sea

To explore the possibility of large-scale CO_2 storage offshore Norway, the Norwegian Petroleum Directorate (NPD) has produced a CO_2 Storage Atlas [15] which considers three different regions that are opened for petroleum activity: the Norwegian part of the North Sea, the Norwegian Sea, and the

Barents Sea. The atlas assesses a large number of geological formations individually and then groups formations into several aquifers whose qualities have been assessed with regard to CO_2 storage potential. Similar atlases have been compiled in other parts of the world, see e.g., [16, 17, 18, 19, 20, 21].

As part of MRST-co2lab, we have implemented functionality that provides simple access to the (GIS formatted) data set published along with the North Sea CO_2 Storage Atlas [22]. The data set includes formation thickness and depth maps that cover vast scales and hence have a spatial resolution of 500–1000 m. Despite the coarse resolution, the data can still be used to provide indicative estimates of the capacity for structural trapping and simulate likely outcomes of specific injection scenarios. To establish a volumetric grid of an aquifer, the minimal required information is a depth map of the top surface and a map of the formation thickness, or equivalents thereof. Not all formations have both a depth and a thickness map, and when both are present, the data sets are not necessarily fully consistent: Coordinates of the depth and thickness maps do not always coincide and sections of the depth map may not be included in the thickness map and vice versa. Using linear interpolation of the thickness maps in regions where the scattered data overlap, we were able to construct volumetric models of fourteen different sand volumes [4]. In the following, we will use the various tools from MRST-co2lab to analyze two of the generated models: the Skade Formation and the Sandnes Formation. These formations are of considerably different character, both in terms of depth, shape and rock properties, and this has to be taken into account when defining and analyzing CO_2 storage scenarios.

3.1. The Skade Formation: capacity estimate

In this section, we estimate the total retaining capacity of the Skade Formation using the approach outlined above. The Skade Formation is considered an open, shallow, and sloping aquifer with regular top surface and very high permeability (more than 1000 mD). It is located off the western coast of Norway, at depths between 450 and 1300 m, with a spatial extent of approximately 100 km in the east–west direction, 270 km in the north–south direction, and a maximum thickness of approximately 300 m. It lies beneath, and is thought to communicate with the Utsira Formation, which we have investigated previously [23, 24] using an approach that is similar to the one we will use herein. The parameter values used to produce the estimates reported below are from [25, 26, 27] and listed in Table 1. These values are

for the Utsira Formation, but in lack of more precise data, we consider these adequate also for the underlying Skade Formation. To compute local CO_2 densities, we use a CO_2 equation-of-state suggested by [28]. Our grid model, reconstructed from the CO_2 Atlas data, has a spatial resolution of 500 m in the lateral directions.

Table 1: Parameter values used to estimate trapping capacities for the Skade Formation.

Parameter	Value	Unit	Reference
Sea depth	80	m	Holloway et al. [26]
Injection depth	1012	m	Singh et al. [25]
Thermal gradient	35.6	°C/km	Singh et al. [25]
Seabed temperature	7	°C	Singh et al. [25]
Residual water saturation	0.11		Singh et al. [25]
Residual CO_2 saturation	0.21		Singh et al. [25]
Rock porosity	0.36		Singh et al. [25]
Water density	1020	kg/m^3	Singh et al. [25]
CO_2 solubility in brine	53	kg/m^3	Chadwick et al. [27]

From these data we estimate the total retaining capacity presented in Table 2. The total theoretical capacity is 63 Gt, of which approximately two thirds are residual and one third is dissolution. Structural trapping capacity (0.43 Gt) constitutes less than one percent of the total. With almost no structural traps (or other caprock morphology) to retard the plume migration, we should therefore expect that a mobile CO_2 plume will migrate relatively fast in the upslope direction.

Table 2: Upper bounds on the trapping capacity in the Skade Formation.

Type	Value [Gt]	% of total
Structural	0.43	0.7
Residual	42.05	66.5
Dissolution	20.79	32.9
Total	63.27	100.0

In the left plot of Figure 5, we visualize the distribution of total retaining capacity across the horizontal domain of the Skade model. We note that the highest capacities are associated with a band in the middle, stretching from north to south. In general, the aquifer grows in thickness towards the middle and the western side, which by itself would mean higher storage capacity.

However, the aquifer is also sloping upwards towards the west, and along the middle we can note a sharp boundary in the data. Left of this line, the aquifer is shallow enough that CO_2 will be in gas phase below the caprock. The very low density of CO_2 in this region means that the corresponding storage capacity will be small. In this study, we have used the density at the level of caprock as representative for the whole column. A more rigorous approach would be to consider variable vertical density, in which case the impact of this boundary would be less.

The positions and storage capacities of structural traps are indicated on the right plot of Figure 5. We recognize three large traps with significantly higher storage capacities than the others. We also note a large trap in the middle of the gas region which, despite its spatial extent, does not provide much in terms of storage capacity due to the low local CO_2 density. An injection strategy aiming to reach structural traps needs to identify injection points that are upward-connected to the large traps. The right plot of Figure 6 displays the total trapping capacity reachable by migration, which for each point in the model is defined as the sum of all traps that are encountered along the spill path originating from this specific point. From this map, we can see that the best places to inject are found in a limited region in the North and in a smaller one in the South. This can be further understood by examining the detailed map of spill-paths in the left plot of Figure 6, which shows explicitly how traps are connected.

3.2. The Skade Formation: injection and migration study

If CCS is to play a significant role in abating European greenhouse gas emission, hundreds of megatonnes of CO_2 will need to be sequestered underground every year. We here aim to design a use case for the Skade formation that will maximize long-term CO_2 storage in the aquifer after an injection period of fifty years. Throughout this exercise, we work on a model with reduced resolution, so that the area of each grid cell is 1.5×1.5 km^2. This is done for convenience, in order to speed up the nonlinear optimization of well rates discussed below, which involves a significant number of separate flow simulations. On the other hand, the procedure could equally be applied on the full-resolution dataset, when higher precision is a priority.

The limited amount of structural traps and the high permeability of this aquifer means that the potential for long-term leakage is significant and needs to be an important guiding factor when designing injection scenarios. Strate-

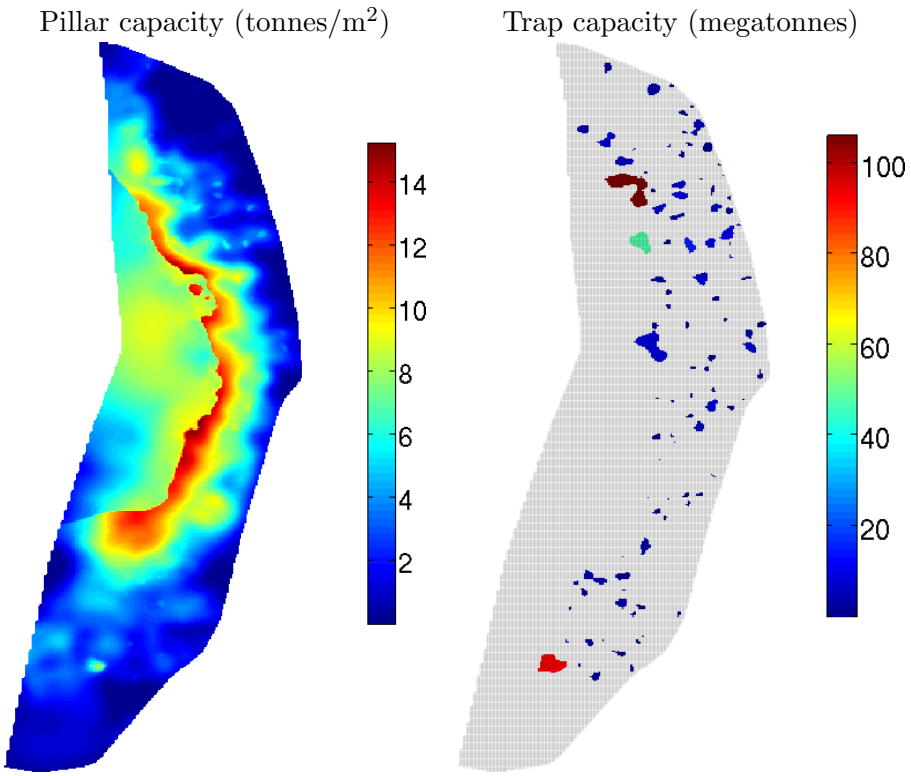

Figure 5: **Left:** Total CO_2 retaining capacity (structural, residual, dissolution) for the Skade model (tonnes per m^2). **Right:** Position and capacity of structural traps (megatonnes per trap).

gic well positioning is necessary to exploit the available structural traps. Moreover, injection should take place as far as possible from the crest of the aquifer to maximize migration time and distance, thus benefiting as much as possible from residual and dissolution trapping mechanisms.

We start by selecting injection sites that maximize the amount of structural capacity reached by gravity-driven migration. To do this, we use the information about the spill system as input to a simple "greedy" algorithm: We pick the lowest leaf node of the spill tree associated with the highest reachable structural capacity, as visualized in the right plot of Figure 5. We place a well as low as possible in the associated catchment area (in practice, we exclude a buffer zone at the perimeter to reduce the chances of CO_2 being pushed out of the intended area during the course of injection). The associated well is then assigned an injection rate designed to inject enough CO_2 to

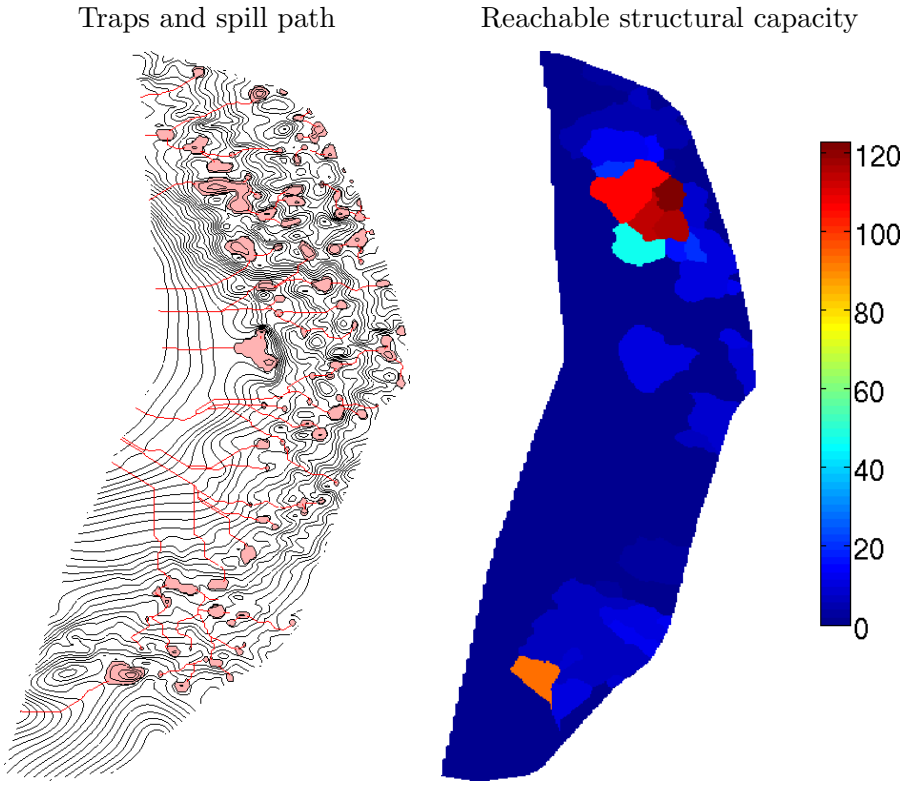

Figure 6: **Left:** Detailed map of spill paths and traps defined by the top surface of the Skade model. **Right:** Combined structural trapping capacity reachable by gravity migration from a given injection point (megatonnes).

fill all the upslope-connected traps within the injection period. To select the next injection point, all traps currently covered are conceptually removed, spill trees are recomputed, and the procedure is run again. The process is repeated until the desired number of well sites have been identified, or until there are no more structural traps to cover.

The result of using the greedy algorithm to select twenty sites for this coarsened aquifer model is presented in the left plot of Figure 7. We note that the five first sites chosen are all associated with the two regions identified in the discussion of Figure 5. Once the large traps are covered, the wells chosen afterwards are scattered all around to cover the remaining trap trees. The corresponding injection rates are presented as blue bars in the right plot of Figure 7. We note a very large spread in injection rates, reflecting the fact that most of the structural capacity is covered already after the first few sites

have been chosen.

The total amount of structural trapping covered by the twenty wells is 309 Mt, which includes practically all the available traps. This amount is less than the capacity identified in Table 2, which is mainly a result of the lower spatial resolution in the top-surface grid. The computation of trapping capacity is highly sensitive to grid resolution, as further examined in [24]. However, for practical simulation purposes, it is possible to compensate for this loss by deriving nonlinear, upscaled phase-mobility functions that partially account for retardation effects induced by CO_2 being trapped in subscale caprock undulations, as discussed in [5]. Henceforth, we refer to this effect (and the corresponding modification of the upscaled phase mobilites) as "subscale trapping".

To evaluate the feasibility and performance of this injection plan, we use a VE simulation to study pressure buildup and the effect of the various trapping mechanisms. We use simulation parameters as presented in Tables 1 and 3, impose Dirichlet boundary conditions corresponding to hydrostatic pressure, and use temperature and pressure-dependent CO_2 properties described by [28]. We include structural, subscale, and residual trapping in the simulation. However, we disregard solubility trapping as there is not yet consensus on how this effect should be modeled on Utsira/Skade system.

From Figure 8 it is clear that pressure buildup will not be a concern for the proposed injection strategy; the highest overpressure is reached towards the beginning of the injection period, for which we observe a maximum overpressure of about 0.7 MPa. This is well below the estimated overburden pressure ranging from 7.8 to 21 MPa across the aquifer, assuming a lithostatic gradient of 17 MPa / 1000 m.

The upper row of Figure 9 presents snapshots of this simulation for selected years, at the end of the injection operation (left) and one thousand years (middle) and three thousand years (right) after injection ceased. A zoom of the southern region after three thousand years gravity-driven migration is shown to the in the second row of the figure. The injected CO_2 gradually migrates from the areas around the injection points and towards the structural traps. However, we note that not all CO_2 reaches its targeted destination, but becomes trapped as residual saturation along the way. This also becomes apparent when we look at the left plot of Figure 10, which presents the different types of trapping that have taken place for the injected CO_2 as a function of time (an explanation of the terminology used is presented in Table 4). In summary, we observe, as expected, that accounting for

the effect of residual trapping allows us to propose an plan that injects more CO_2 than what was feasible when considering structural capacity alone.

To take further advantage of residual trapping and maximize the storage potential from our selected injection sites, we aim to optimize injection rates. To this end, we employ a nonlinear optimization algorithm based on a steepest descent method with gradients computed numerically by an adjoint method as part of the simulation, facilitated by automatic differentiation. For robustness, dynamic time-stepping is implemented and constraints are handled by projections, see [12] for details. As our objective function, we will use:

$$J(t) = M^i(t) - C\big[M^i(t) - M^a(t)\big], \tag{10}$$

where M^i is the total injected mass of CO_2 and M^a is the mass of CO_2 that is currently present within the aquifer. In other words, we seek to maximize the injected CO_2 mass and minimize the mass that leaves across aquifer boundaries, using a weighting factor C. By setting $C = 10$, the objective function becomes negative if more than 10% of the injected CO_2 is allowed to escape across the perimeter of the aquifer.

After the optimization procedure, we obtain the wellrates shown as red bars in the plot to the right in Figure 7. Comparing with the previous values (blue), we see that most rates have been adjusted upwards. Most notably, wells number 12, 14, 15, and 16 now have significantly increased rates. These wells, which were of marginal importance when only structural trapping was taken into account, have now been attributed injection rates making them a much more significant part of the total figure. From the left plot of the same figure, we see that these wells are all situated in the deep, south-eastern end of the aquifer, where CO_2 will migrate upwards for long distances towards Northwest, continuously losing mass because of residual trapping, but undisturbed by migrating plumes from neighboring injection sites. A corresponding snapshot of the southern region at the end of the simulation is presented in the bottom middle diagram of Figure 9. The traps are now mostly filled by the plumes, and we also see a large footprint of residual CO_2 in the regions through which CO_2 has migrated. The CO_2 trapping distribution is presented in the middle plot of Figure 10. We note that the optimization procedure enables us to increase the total amount of injected CO_2 to 392 Mt.

Data from the simulation shows that a total of 661 Mt of water was expelled from the aquifer during injection and migration. Whereas we have

used open boundaries in our simulation, a more complete model would also take into account how this water is likely to be redistributed in neighboring formations or discharged from the sea floor. For this study, however, we had no data that would allow us to make a qualified hypothesis on the matter.

A similar study was carried out for the Utsira Formation in [24, 23]. In that study, residual trapping played a larger role in the final CO_2 inventory. This appears to be related to the significantly larger plumes injected, as total structural capacity of that formation proved to be 2.6 times higher than for Skade. The larger and taller plumes lead to more swept volumes and hence a larger amount of residual trapping realized. While not yet studied in detail, this suggest that a difference in structural capacity between two otherwise similar aquifers could yield a significantly larger difference in realized trapping capacity due to the additional residual trapping reached during migration.

Finally, in to illustrate the potential impact of solubility trapping on achievable storage capacity for the Skade Formation, we rerun the simulation with identical injection rates, but now include the effect of dissolution. For CO_2 solubility in brine, we use the value presented in Table 1, and consider a dissolution rate of 0.44 kg/m^2/year. A snapshot of the southern region at the end of the simulation is shown at the bottom-right diagram of Figure 9. After three thousands years of post-injection migration, there is little left of the injected plumes and only two traps are (partially) filled. Most of the injected CO_2 is found in dissolved state. Dissolution has also limited the spatial extent of migration, as can be seen by comparing with the case without dissolution. The corresponding CO_2 inventory is presented in the right plot of Figure 10. Again, we see that for the chosen parameters, dissolution quickly becomes the dominant effect. Although actual dissolution rates are not known for the Skade Formation, it is clear that an effect of this magnitude will have large implications for the realizable storage capacity of the aquifer.

3.3. The Sandnes Formation

Among all the data sets extracted from the North Sea CO_2 Storage Atlas [22], the Sandnes Formation is the aquifer that has the highest potential of structural trapping thanks to a combination of many medium-sized traps and several huge domes that may potentially store large amounts of CO_2. Out of a total bulk volume of 1550 Gm^3, approximately 213 Gm^3 (or 14%) fall inside what can be characterized as structural traps. Repeating the same storage

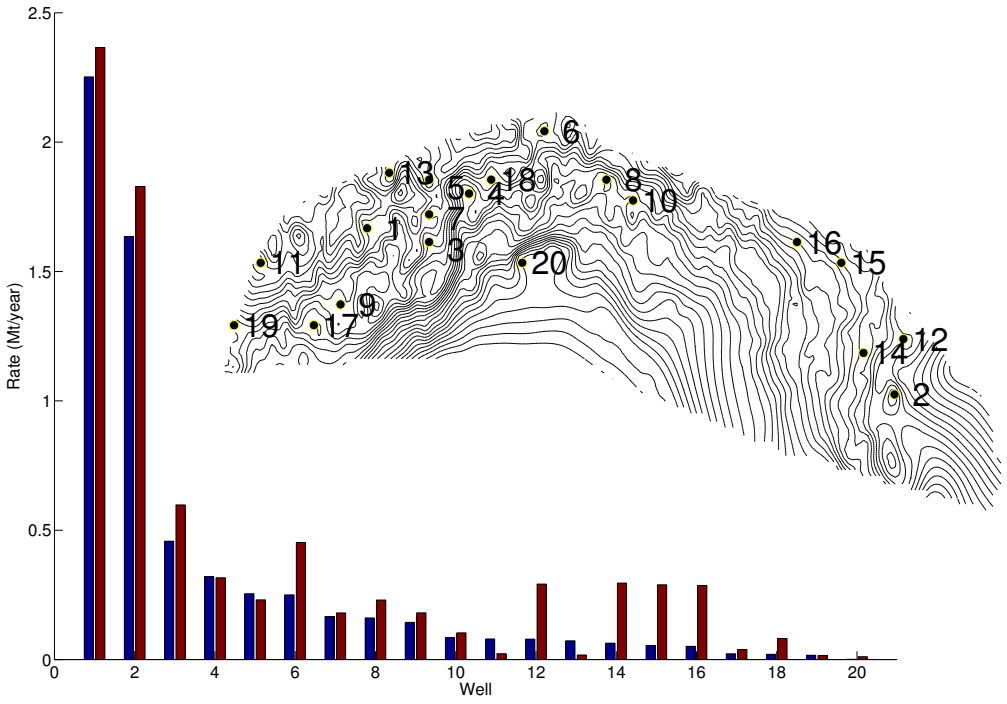

Figure 7: Optimization of the injection scenario for the Skade model. Injection sites are determined by the "greedy" algorithm and numbered according to the order chosen. The blue bars represent initially chosen rates, and red bars optimized rates.

Table 3: Simulation parameter values used to optimize injection scenarios.

Parameter	Value	Unit	Reference
Injection period	50	year	
Migration period	3000	year	
brine viscosity	$8 \cdot 10^{-4}$	Pa· s	Singh et al. [25]
CO_2 viscosity	$6 \cdot 10^{-5}$	Pa· s	Singh et al. [25]
rock permeability	2	Darcy	Singh et al. [25]
brine compressibility	4.3×10^{-5}	bar^{-1}	(ref. pressure: 10 MPa)
rock compressibility	1.0×10^{-5}	bar^{-1}	(ref. pressure: 10 MPa)

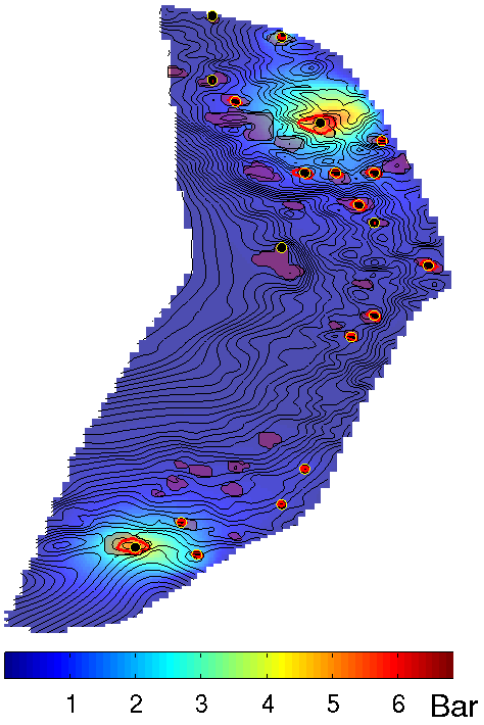

Figure 8: Overpressure in the Skade aquifer five years into the injection operation.

Table 4: The terminology used in the CO_2 inventories in Figures 10 and 11.

State	Explanation
Dissolved	CO_2 trapped by dissolution into formation brine
Structural residual	CO_2 that is both structurally and residually trapped
Residual	Residually trapped CO_2 outside plume and structural traps
Residual in plume	CO_2 still in the free-flowing plume, but destined to be left behind
Structural subscale	CO_2 trapped in caprock structures too small to be represented by the grid
Structural plume	structurally trapped CO_2, other than "structural residual"
Free plume	CO_2 that is still free to migrate
Exited	CO_2 that has left the simulated domain

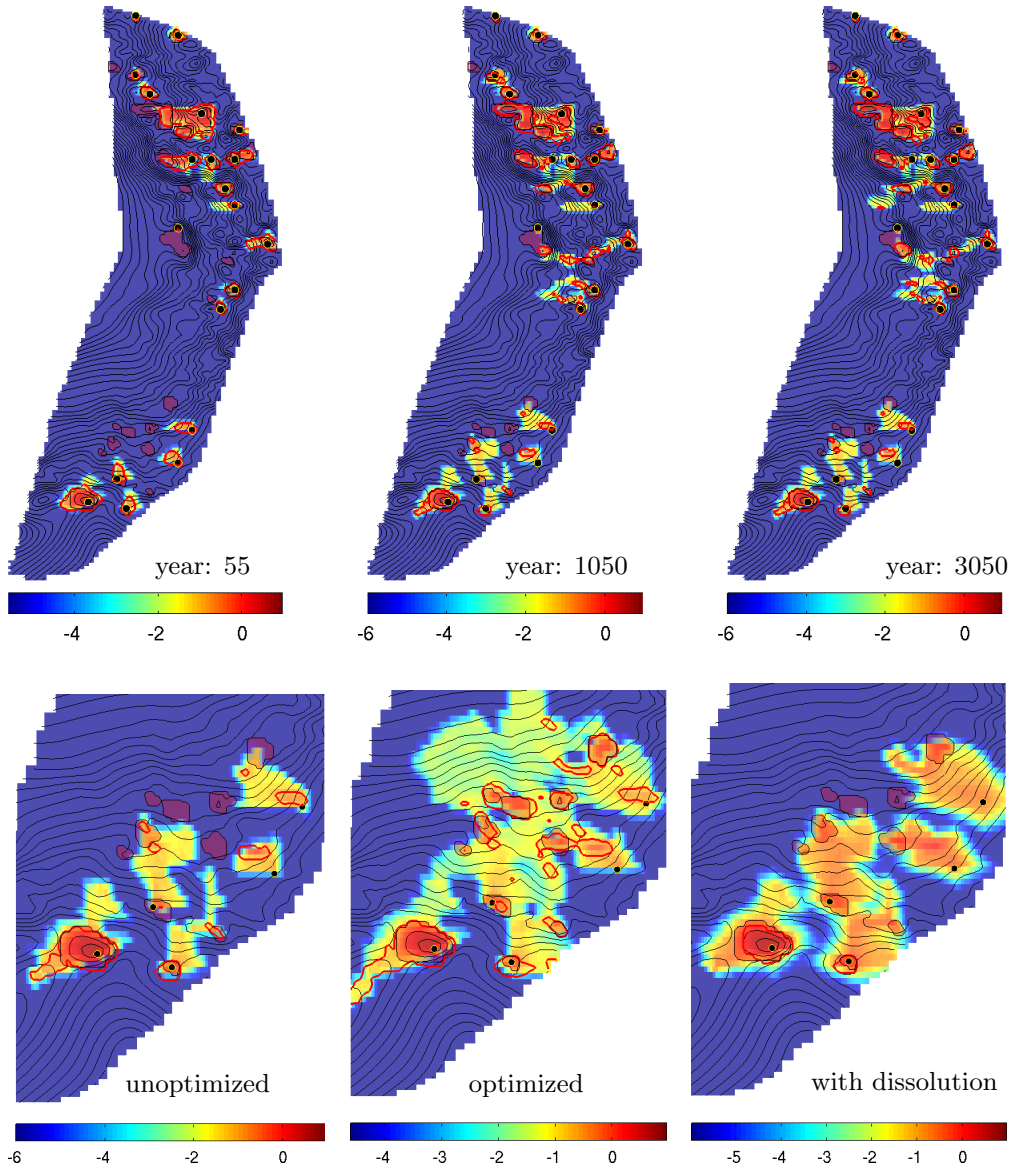

Figure 9: Simulation of CO_2 injection and migration in the Skade Formation: CO_2 plume outlined in red, structural traps overlaid in purple. Total vertical integrated CO_2 content indicated with color (unit: tonnes per lateral square meter, logarithmic scale with base 10). Wells are indicated with black circles. **Upper row:** Simulation of unoptimized case, snapshots for selected years. **Bottom row:** Zoom of the southern region after 3050 years for the unoptimized case (left), the case with optimized well rates (middle), and the case with optimized well rates and dissolution effects during migration (right).

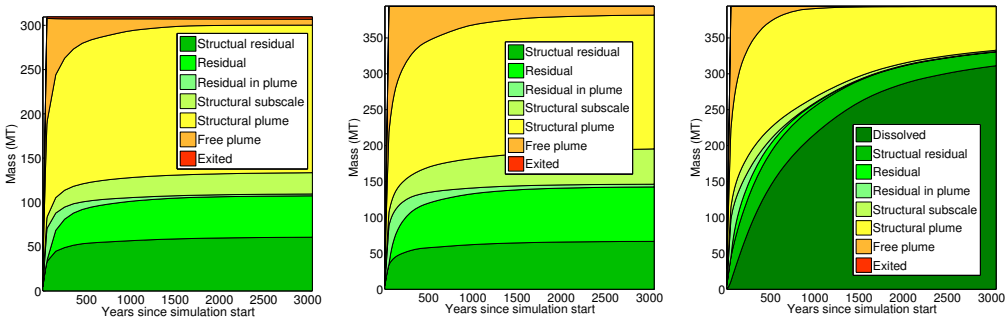

Figure 10: Detailed CO_2 inventories for three different large-scale injection and long-time migration scenarios for the Skade Formation: simulation of default case (left), simulation with optimized well rates (middle), and simulation with optimized well rates and plausible dissolution effects (right).

capacity analysis as for the Skade Formation indicates that the upper bound on the storage capacity is 24 Gt of CO_2, distributed as 9 Gt in structural traps, 14 Gt residually trapped, and 1 Gt dissolved into the formation water. On the other hand, outside local depocenters most of the Sandnes Formation is relatively thin (50 m or less) and the estimated permeability ($\sim$150 mD) is significantly lower than for the Skade Formation. This suggest that pressure buildup might quickly become an issue.

Because of the very large trap volumes that potentially can be filled, we revise the greedy algorithm introduced above slightly, so that each well that is initially assigned a rate larger than 5 Mt/year is split into multiple wells scattered within the same catchment area. From this, we obtain an injection plan that seeks to inject 10 Gt within a period of fifty years, which is an overly optimistic and not very realistic plan. As shown in Figure 11, several clusters of wells will try to inject very large volumes into relatively small regions. Such an injection is obviously not realizable in real life, and in our numerical simulation we also observe a completely unrealistic pressure buildup that will force large volumes of CO_2 out across the perimeter of the aquifer. (For the simulation, we used the same fluid parameters as for the Skade Formation, but with a temperature of 85° C.)

For this formation, we will therefore try a different strategy for the placement of injection hubs. We start by distributing forty-seven hubs relatively uniformly throughout the aquifer, as illustrated in the left plot of Figure 12. Second, we modify the objective function (10) so that the present mass is only computed inside catchment areas that do not spill to the boundary (i.e.,

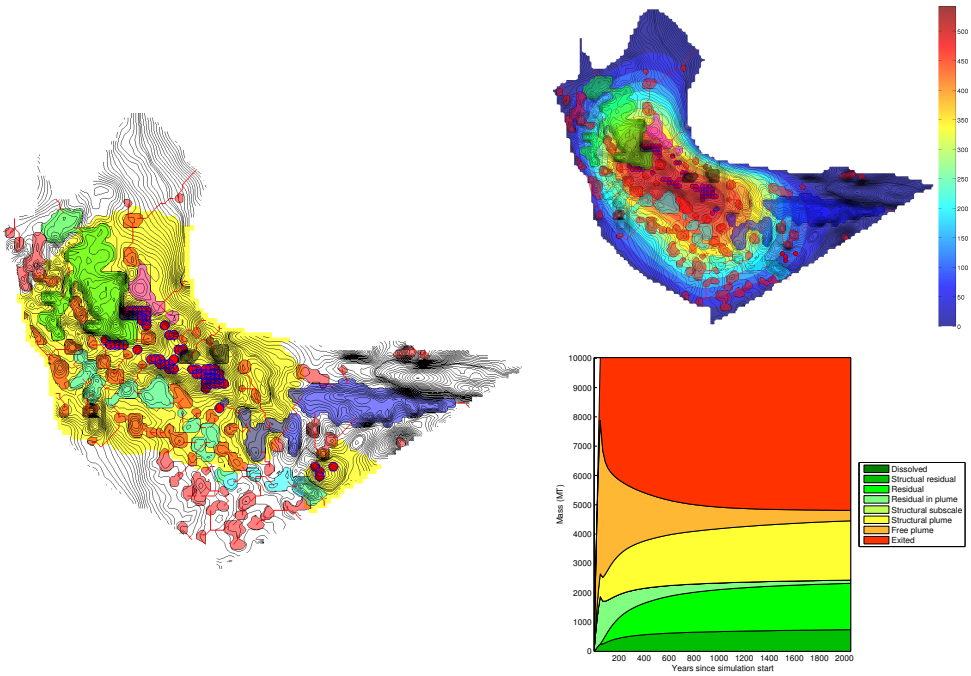

Figure 11: **Left:** Distribution of potential injection hubs in the Sandnes Formation suggested by greedy optimization of the spill system. Circles indicate wells, the five largest spill trees have a unique color, the remaining are shown in red, and yellow color is the plume after fifty years. **Upper right:** The pressure increase in units bar at the end of the injection period. **Lower right:** Detailed inventory of the volumetric CO_2 distribution as a function of time.

cells that are within the green region in the right plot of Figure 12).

Constraining the objective function by the catchment areas as explained above suggests a constant-rate strategy that will inject a total of 2.5 Gt. The outcome of this strategy is that more than 50% of the injected volume ends up inside a single connected plume that covers a large fraction of the top surface and is expanding outward, as shown on the left in Figure 13. The fact that the plume is expanding can be seen since no residual trapping has taken place outside of the structural traps. This outcome is still not feasible in a long-term perspective because the height of the plume and the pressure inside will cause it to continue expanding, which will move significant amounts of CO_2 into the spill region associated with the boundary.

To overcome this problem, we allow the optimization algorithm to specify a time-varying rate and maximize the objective function (10) one hundred

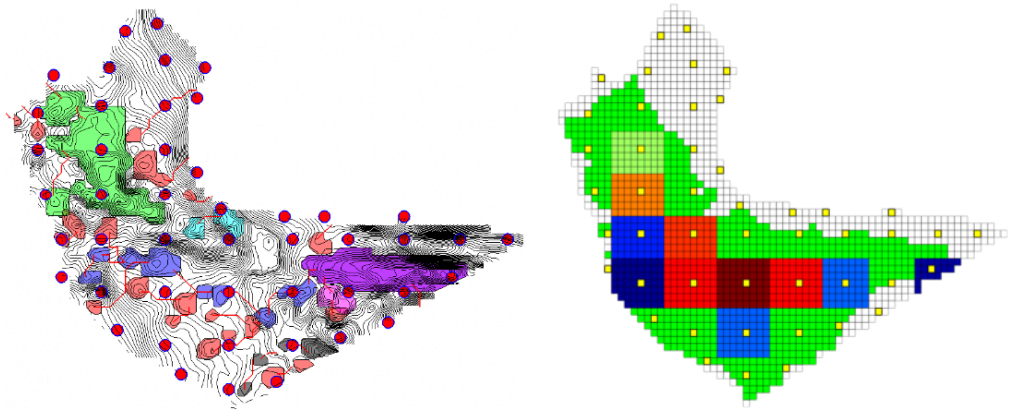

Figure 12: Constrained optimization of injection strategy for the Sandnes Formation. **Left:** A regular coarse partition (from the coarsegrid module of MRST) is imposed on the top surface grid and a well is place at the center of each coarse block. **Right:** Green color signifies catchment areas that do not spill to the perimeter of the aquifer. The colors of the blocks indicate the rate of the corresponding well after optimization with constant rate.

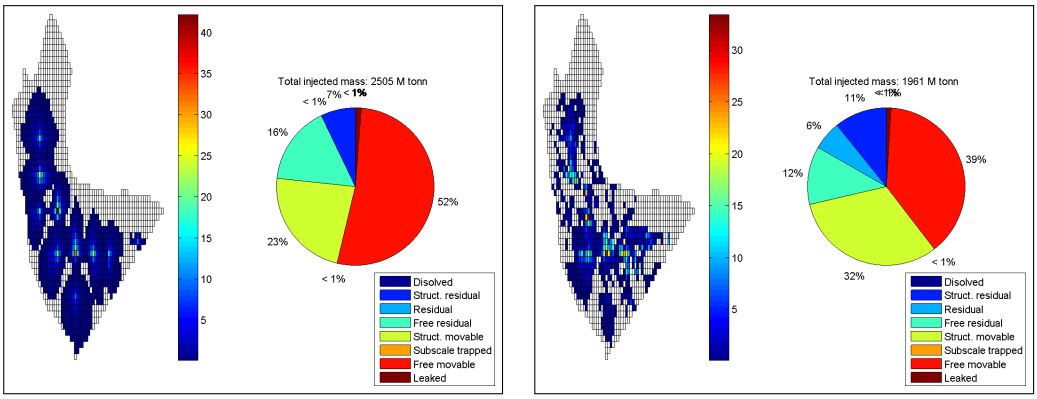

Figure 13: Distribution of CO_2 in the Sandnes Formation at the end of injection. The pie charts show the inventory of the CO_2, while the grid plots show the height of the CO_2 column for each cell in the VE model. **Left:** Injection strategy derived by maximizing the value of the objective function (10) at the end of the injection period. **Right:** Alternative strategy suggested by maximizing the value of the objective function 100 years after the injection has stopped.

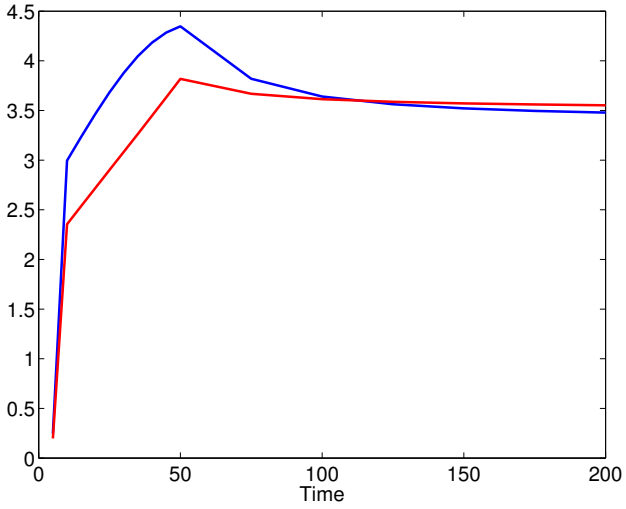

Figure 14: Objective function (10) as function of time for two different injection strategies: Blue line denotes a constant rate strategy that has been optimized over the injection period of fifty years, whereas the red line denotes a variable rate strategy that has been optimized up to one hundred years after the injection has ceased.

years after the injection has stopped. By then, the dynamics of the plume has switched from being viscous dominated to being driven by buoyancy forces, and the objective function will have more time to penalize leakage. In the resulting strategy, 1.9 Gt is injected. The right plot in Figure 13 shows that with the new strategy, the movable plume is significantly reduced, and that unlike in the previous case, residual trapping has taken place already during the injection period. Figure 14 shows the objective function for the two different injection strategies. Here we see that the constant-rate strategy attains a high value at the end of simulation by pushing a lot of CO_2 into the domain. However, during the migration phase the objective function decreases due to leakage across the boundary. The second strategy injects a smaller quantity and therefore attains a lower value at the end of injection, but causes less leakage across the boundary and will therefore experience less drop-off in the long perspective.

4. Concluding remarks

Accurate modeling and optimization of CO_2 storage operations is a challenging multiscale problem. The choice of modeling scale and computational

approach will to a large extent depend on the type of questions asked and the characteristics of the aquifer in question, and to be able to provide answers that are trustworthy, the successful modeler should have a large toolbox of models and computational methods of varying fidelity and computational complexity.

Whereas traditional 3D simulation tools are indispensable to study problems on a mesoscopic scale (injectivity, early formation of the 3D plume, pressure buildup and thermo-mechanical effects in the near-well zone, etc), they generally fall short if the focus is on the large-scale, long-term distribution of injected volumes. For this type of problem, combinations of simple geometrical methods borrowing ideas from hydrology and basin modeling with vertically integrated models formulated on a 2D grid that follows the top surface of an aquifer, constitute a powerful approach. Such methods can be used to efficiently delineate structural traps and migration paths and simulate the likely outcomes of injection scenarios, in order to provide estimates of structural, residual, and solubility trapping. As a general rule, we strongly advice that this type of models and methods are used early in the modeling workflow to efficiently investigate alternative hypotheses and explore as much as possible of parameter space to accurately span the range of likely outcomes.

In this paper, we have briefly outlined a set of geometrical tools and VE simulation models that have been implemented as a separate module, MRST-co2lab, in the open-source MATLAB Reservoir Simulation Toolbox (MRST). Apart from a rapid development cycle in MATLAB compared with compiled languages, the main purpose of using MRST is to make the new methods interoperable with the wide range of traditional 3D modeling tools that are already implemented in the software. To this end, the methods in MRST-co2lab have mainly been developed using unified data models and modeling frameworks inherited from commercial reservoir simulators. Altogether, we believe that the software is a good platform for conducting reproducible research on models and methods of industry-standard complexity.

In the main part of the paper we have demonstrated how the various functionality in MRST-co2lab can be combined in a two-level workflow for developing optimized injection plans: In the first phase, estimates of structural traps and spill paths are used to determine injection locations optimal in terms of residual trapping and reduced risk for leakage through the boundary. Then, these injection points are used as an initial guess in a rigorous mathematical optimization of injection rates that uses and adjoint formu-

lation that can be efficiently realized using automatic differentiation. The actual numbers presented in our paper are based on limited data and therefore serve mainly to illustrate the usefulness of the underlying computational methods and *should not* be taken literally as true estimates of actual storage capacities. To provide realistic estimates, one would need to include a better description of the many parameters and physical effects that enter our models. For petrophysical parameters we used a single average value, we have assumed constant CO_2 density throughout individual vertical columns, dissolution rates are highly uncertain, etc. Moreover, for the two cases considered herein, all wells were constrained by rate only. In a more realistic setting, wells would be constrained by pressure, or by a combination of rate and pressure constraints. In particular, there would be important pressure constraints around the wells during the injection period to avoid threatening caprock integrity. Also, formation water will not likely just disappear across open boundaries (as tacitly assumed in our analysis). Expelled brine volumes will most likely contribute to further increase in pressure, which will further tighten constrains on injection rates and volumes, and might be included in the objective function. While all these effects will make the optimization problem harder to solve (e.g., if wells switch between rate and pressure constraints), our forward simulators should still provide accurate gradients that can be fed into existing optimization methods developed for petroleum applications.

Finally, we believe that the combination of spill-point analysis and vertical-equilibrium simulations represents an effective means for exploring alternative assumptions and hypotheses to develop a better understanding of the problem and its associated uncertainty, figure which effects are important and which can likely be neglected, exclude blind alleys, and so on, before diving into more comprehensive modeling and simulation frameworks. If nothing else, this is how we prefer to approach the challenging problem of CO_2 storage.

5. Acknowledgments

The work was funded in part by Statoil ASA and the Research Council of Norway through grants no. 199878 (Numerical CO_2 laboratory) and 215641 (MatMoRA-II).

References

References

[1] The MATLAB Reservoir Simulation Toolbox, version 2014a, http://www.sintef.no/MRST/ (May 2014).

[2] K.-A. Lie, S. Krogstad, I. S. Ligaarden, J. R. Natvig, H. M. Nilsen, B. Skaflestad, Open source MATLAB implementation of consistent discretisations on complex grids, Comput. Geosci. 16 (2012) 297–322. doi:10.1007/s10596-011-9244-4.

[3] SINTEF ICT, The MATLAB Reservoir Simulation Toolbox: Numerical CO_2 laboratory (Oct. 2014).
URL http://www.sintef.no/co2lab

[4] H. M. Nilsen, K.-A. Lie, O. Møyner, O. Andersen, Spill-point analysis and structural trapping capacity in saline aquifers using MRST-co2lab, Computers & Geoscience 75 (2015) 33–43. doi:10.1016/j.cageo.2014.11.002.

[5] H. M. Nilsen, K.-A. Lie, O. Andersen, Robust simulation of sharp-interface models for fast estimation of CO_2 trapping capacity.
URL http://folk.uio.no/kalie/papers/co2lab-2.pdf

[6] H. M. Nilsen, K.-A. Lie, O. Andersen, Fully implicit simulation of vertical-equilibrium models with hysteresis and capillary fringe.
URL http://folk.uio.no/kalie/papers/co2lab-3.pdf

[7] S. E. Gasda, J. M. Nordbotten, M. A. Celia, Vertical equilibrium with sub-scale analytical methods for geological C02 sequestration, Comput. Geosci. 13 (4) (2009) 469–481. doi:10.1007/s10596-009-9138-x.

[8] H. M. Nilsen, P. A. Herrera, M. Ashraf, I. Ligaarden, M. Iding, C. Hermanrud, K.-A. Lie, J. M. Nordbotten, H. K. Dahle, E. Keilegavlen, Field-case simulation of CO2-plume migration using vertical-equilibrium models, Energy Procedia 4 (0) (2011) 3801–3808. doi:10.1016/j.egypro.2011.02.315.

[9] S. E. Gasda, J. M. Nordbotten, M. A. Celia, Vertically-averaged approaches to CO2 injection with solubility trapping, Water Resources Research 47 (2011) W05528. doi:10.1029/2010WR009075.

[10] S. E. Gasda, H. M. Nilsen, H. K. Dahle, W. G. Gray, Effective models for CO_2 migration in geological systems with varying topography, Water Resour. Res. 48 (10). doi:10.1029/2012WR012264.

[11] F. Doster, J. M. Nordbotten, M. A. Celia, Hysteretic upscaled constitutive relationships for vertically integrated porous media flow, Comput. Visual. Sci. 15 (2012) 147–161. doi:10.1007/s00791-013-0206-3.

[12] X. Raynaud, S. Krogstad, H. M. Nilsen, Reservoir management optimization using calibrated transmissibility upscaling, in: ECMOR XIV – 14^{th} European Conference on the Mathematics of Oil Recovery, Catania, Sicily, Italy, 8-11 September 2014, EAGE, 2014. doi:10.3997/2214-4609.20141864.

[13] S. Krogstad, K.-A. Lie, O. Møyner, H. M. Nilsen, X. Raynaud, B. Skaflestad, MRST-AD – an open-source framework for rapid prototyping and evaluation of reservoir simulation problems, in: SPE Reservoir Simulation Symposium, 23–25 February, Houston, Texas, 2015. doi:10.2118/173317-MS.

[14] R. Neidinger, Introduction to automatic differentiation and MATLAB object-oriented programming, SIAM Review 52 (3) (2010) 545–563. doi:10.1137/080743627.

[15] E. K. Halland, J. Mujezinović, F. Riis (Eds.), CO_2 Storage Atlas: Norwegian Continental Shelf, Norwegian Petroleum Directorate, P.O. Box 600, NO-4003 Stavanger, Norway, 2014.
URL `http://www.npd.no/en/Publications/Reports/Compiled-CO2-atlas/`

[16] D. Lewis, et al., Assessment of the potential for geological storage of carbon dioxide for the island of Ireland, Tech. rep., Sustainable Energy Ireland, Environmental Protection Agency, Geological Survey of Northern Ireland, and Geological Survey of Ireland (2008).

[17] D. Lewis, M. Bentham, T. Cleary, R. Vernon, N. ONeill, K. Kirk, A. Chadwick, D. Hilditch, K. Michael, G. Allinson, P. Neal, M. Ho,

Assessment of the potential for geological storage of carbon dioxide in Ireland and Northern Ireland, Energy Procedia 1 (1) (2009) 2655–2662. doi:10.1016/j.egypro.2009.02.033.

[18] Natural Resources Canada, Mexican Ministry of Energy, and U.S. Department of Energy, The North American Carbon Storage Atlas (2012). URL http://www.nacsap.org/

[19] U. S. Department of Energy, Office of Fossil Energy, The 2012 United States Carbon Utilization and Storage Atlas, 4th Edition (2012). URL http://www.netl.doe.gov/research/coal/carbon-storage/atlasiv

[20] M. Cloete, Atlas on geological storage of carbon dioxide in South Africa, Tech. rep., Council for Geoscience, Johannesburg, South Africa (2010). URL http://www.sacccs.org.za/wp-content/uploads/2010/11/Atlas.pdf

[21] B. E. Bradshaw, L. K. Spencer, A.-L. Lahtinen, K. Khider, D. J. Ryan, J. B. Colwell, A. Chirinos, J. Bradshaw, J. J. Draper, J. Hodgkinson, M. McKillop, An assessment of Queensland's CO2 geological storage prospectivity–The Queensland CO2 geological storage atlas, Energy Procedia 4 (0) (2011) 4583–4590. doi:10.1016/j.egypro.2011.02.417.

[22] E. K. Halland, W. T. Johansen, F. Riis (Eds.), CO_2 Storage Atlas: Norwegian North Sea, Norwegian Petroleum Directorate, P. O. Box 600, NO–4003 Stavanger, Norway, 2011. URL http://www.npd.no/no/Publikasjoner/Rapporter/CO2-lagringsatlas/

[23] O. Andersen, H. M. Nilsen, K.-A. Lie, Reexamining CO_2 storage capacity and utilization of the Utsira Formation, in: ECMOR XIV – 14^{th} European Conference on the Mathematics of Oil Recovery, Catania, Sicily, Italy, 8-11 September 2014, EAGE, 2014. doi:10.3997/2214-4609.20141809.

[24] H. M. Nilsen, K.-A. Lie, O. Andersen, Analysis of trapping capacities in the Norwegian North Sea using MRST-co2lab, Computers & Geoscience 79 (2015) 15–26. doi:10.1016/j.cageo.2015.03.001.

[25] V. Singh, A. Cavanagh, H. Hansen, B. Nazarian, M. Iding, P. Ringrose, Reservoir modeling of CO_2 plume behavior calibrated against moni-

toring data from Sleipner, Norway, in: SPE Annual Technical Conference and Exhibition, 19-22 September 2010, Florence, Italy, 2010, SPE 134891-MS. doi:10.2118/134891-MS.

[26] S. Holloway, A. Chadwick, E. Lindeberg, I. Czernichowski-Lauriol, R. Arts, Best practice manual from SACS–Saline aquifer CO2 storage project, Tech. rep., Statoil Research Center, Trondheim, Norway, IEA Greenhouse Gas R&D Programme, Schlumberger Research, European Commission (2004).

[27] A. Chadwick, R. Arts, C. Bernstone, F. May, S. Thibeau, P. Zweigel, Best practice for the storage of CO2 in saline aquifers – Observations and guidelines from the SACS and CO2STORE projects, Vol. 14 of British Geological Survey Occasional Publication, British Geological Survey, Nottingham, UK, 2008.
URL `http://nora.nerc.ac.uk/2959/`

[28] R. Span, W. Wagner, A new equation of state for carbon dioxide covering the fluid region from triple-point temperature to 1100 K at pressures up to 800 MPa, J. Phys. Chem. Ref. Data 25 (6) (1996) 1509–1597.